

# Lawrence Berkeley National Laboratory

## Recent Work

### Title

THE ENHANCEMENT OF STRENGTHENING DISLOCATED MARTENSITE

### Permalink

<https://escholarship.org/uc/item/6j28j4m9>

### Authors

Cheng, I-lin

Thomas, G.

### Publication Date

1971-04-01

RECEIVED  
RADIATION LABORATORY

DOCUMENTS SECTION

THE ENHANCEMENT OF STRENGTHENING  
DISLOCATED MARTENSITE

I-lin Cheng and G. Thomas

April 1971

AEC Contract No. W-7405-eng-48

TWO-WEEK LOAN COPY

*This is a Library Circulating Copy  
which may be borrowed for two weeks.  
For a personal retention copy, call  
Tech. Info. Division, Ext. 5545*



25

## **DISCLAIMER**

This document was prepared as an account of work sponsored by the United States Government. While this document is believed to contain correct information, neither the United States Government nor any agency thereof, nor the Regents of the University of California, nor any of their employees, makes any warranty, express or implied, or assumes any legal responsibility for the accuracy, completeness, or usefulness of any information, apparatus, product, or process disclosed, or represents that its use would not infringe privately owned rights. Reference herein to any specific commercial product, process, or service by its trade name, trademark, manufacturer, or otherwise, does not necessarily constitute or imply its endorsement, recommendation, or favoring by the United States Government or any agency thereof, or the Regents of the University of California. The views and opinions of authors expressed herein do not necessarily state or reflect those of the United States Government or any agency thereof or the Regents of the University of California.

THE ENHANCEMENT OF STRENGTHENING DISLOCATED MARTENSITE

I-lin Cheng\* and G. Thomas

Department of Materials Science and Engineering, College of Engineering  
University of California, Berkeley, California

ABSTRACT

The basis of this work was the investigation of improving the tensile properties of dislocated martensites by dispersion of precipitates in the austenite prior to the martensite transformation. Two types of precipitation hardenable austenitic alloys were used. One is based on Fe-22Ni-4Mo-0.28C where the precipitates are  $\text{Mo}_2\text{C}$  and are obtained by ausforming and aging, and the other is Fe-28Ni-2Ti where the precipitates are the coherent FCC  $\gamma'$  ( $\text{Ni}_3\text{Ti}$ ) ordered phase obtained by ausaging.

After the austenitic dispersion treatment both alloys were transformed to martensite by quenching to liquid nitrogen and the properties measured and compared to martensites obtained by conventional heat treatment (i.e. no precipitates in austenite). The results show that prior dispersions increase the strength of martensite and this is interpreted as being due to an increase in dislocation density resulting from dislocation multiplication at the particles during the  $\gamma \rightarrow \text{Ms}$  transformation.

In addition, the stabilities of the austenitic alloys are such that upon certain aging treatments, the alloys transform partially to martensite (due to precipitation) and "composite" materials are obtained whose strength depends on the volume fraction and yield strengths of the phases present.

\* Presently at Borg-Warner Corporation, Des Plaines, Illinois 60018.

## I. INTRODUCTION

Processes for obtaining high strength steels involve various thermal and thermal-mechanical treatments, e.g. ausforming, which eventually produce martensitic structures. However, apart from ausforming, little is known about the origin and character of the substructure of the martensite produced by other complex processes and its relation to mechanical properties. This paper explores this problem and ways of duplicating the benefits of ausforming without requiring plastic deformation as a stage in the process. It is useful first to review what is known about ausforming.

Ausforming is a thermomechanical treatment, whereby the metastable austenite is deformed at elevated temperatures before isothermal decomposition takes place and then cooled to allow the martensite transformation to occur. The mechanical properties of ausformed martensite in steels containing carbon and carbide forming elements, are in general superior to those obtained by conventionally heat treated martensite, for example, the tensile strength may be increased by as much as 30% with generally an improvement in ductility.<sup>1-10</sup>

It has been shown that carbides are formed during deformation of metastable austenite, e.g. by direct observations using electron microscopy<sup>1,2</sup> and indirectly from the observed increase in Ms temperature.<sup>8</sup> These carbides may pin the dislocations in austenite so that they are not likely to be swept away by the advancing martensite boundaries on subsequent martensitic transformation. Consequently, the dislocations may be retained in the resulting martensitic structure.

The martensite transformation itself generates dislocations and by interaction and multiplication at the carbides the total dislocation density can be very high compared to normal martensites. This applies, provided the transformation shear is slip and not twinning. The resulting high dislocation densities have been suggested to account for the improved mechanical properties.<sup>2</sup>

It appears, therefore, that strong tough martensites require conditions favorable to maximising their dislocation density. Control of composition is essential in order to ensure the formation of dislocated martensite, viz. that the concentration of carbon and other alloying elements in austenite just prior to the  $\gamma$ - $\alpha$  transformation is low enough<sup>11</sup> (e.g. carbon < 0.3%). In the case of ausforming the austenite is diluted by deformation of the metastable austenite. The question then of maximising the dislocation density is one of maximising dislocation multiplication during transformation. As is well known from dispersion hardening, precipitate particles are very effective in causing dislocation multiplication during plastic flow and since the  $\gamma$ - $\alpha$  martensite transformation is a special type of plastic deformation and which produces uniform but dense dislocation distributions, it is suggested that dispersion strengthening austenite followed by phase transformation to dislocated martensite might produce the maximum effects of substructural strengthening.

Although these features can be obtained through ausforming,<sup>1,2</sup> in practice the process is lengthy and expensive and for maximum effect requires large amounts of plastic deformation, e.g. in H-11 steel<sup>9,11</sup> the strength is raised by about 1000 to 1300 psi per % deformation.

Consequently it is desirable to duplicate the benefits of ausforming but ideally with a single heat treatment process and without plastic deformation.

Two types of alloys were used in this research. The first one was based on an ausformable alloy of Fe-22Ni-4Mo-0.28C which had been studied earlier.<sup>1,2</sup> This alloy was deformed in the austenitic condition and subsequently recovered or recrystallized in an attempt to reduce the dislocation density but retain the carbides. The "recovered" austenite was then quenched to martensite and compared with the normal ausformed martensite, in order to test the basic hypothesis regarding the role of particles in enhancing dislocation multiplication.

The second type was an Fe-28Ni-2Ti alloy, where proper aging of the austenite (ausaging) is known to produce precipitation of  $\gamma'$  ( $\text{Ni}_3\text{Ti}$ ) particles.<sup>12</sup> The microstructure and mechanical properties of the martensite quenched from ausaged specimens were then analysed in order to help understand the role played by precipitates or particles during the martensitic transformation. During the investigation mixtures of austenite and martensite were obtained after certain aging treatments. This phenomenon was related to the stability of austenite. Since  $M_s$  temperature is known to be depressed by nearly all alloying elements except Co, the depletion of solute atoms from the matrix by precipitation should generally raise the  $M_s$  temperature (see e.g. ref. 14). Consequently, martensite should form partially after cooling to room temperature. The resulting mixed-phase structure would provide an interesting aspect. Work done on 304 stainless steel<sup>15</sup> has shown that the yield strength of a mixture of martensite and austenite was linearly

proportional to the amount of martensite regardless of what kind of treatment was performed to form it. In the present case, because both the martensitic and austenitic phases were strengthened sub-structurally, e.g. by dislocations and precipitates, it is of interest to determine the effect of these strengthening parameters (work hardening, precipitation hardening, etc.) on the overall yield strength attainable of such "composites" as a function of the amount of martensite.

## II. EXPERIMENTAL PROCEDURES\*

### A. Material

Two types of alloy containing Mo and Ti respectively were used in this study. For the sake of convenience, the Mo containing alloy is assigned as Type I alloy and the Ti alloy as Type II. Table I lists their chemical compositions. Type II alloy was kindly supplied by International Nickel Company through Dr. J. R. Mihalisin.

TABLE I Chemical Composition of Alloys (Wt.%)

	Fe	Ni	Mo	Ti	C
Type I	bal	21.67	4.11	---	0.24
Type II	bal	27.69	---	2.01	0.005

### B. Thermal and Mechanical Treatments

#### (1) Type I alloy:

The ingot was cast in a vacuum melting furnace. It was homogenized first at 1250°C for three days and rolled to 0.125" thick blank after reheating to 1000°C. The rolled sheets were then annealed at 1200°C for two hours and ausformed by heating in a 500°C furnace followed immediately by 30% reduction in thickness. The products were water-quenched after

---

\* Complete experimental details are available in UCRL rep. 19196 (Ph. D. thesis, I-L. Cheng).

rolling. Tensile test sheet specimens and coupons for measuring Ms temperatures, x-ray diffraction and transmission electron and optical microscopy were machined from the ausformed sheets.

The samples were vacuum-sealed in quartz tubes for subsequent annealing treatments at temperatures of 500°C and 600°C respectively. Martensitic structures were obtained by quenching the annealed specimens into liquid nitrogen.

(2) Type II alloy:

The materials were received as hot-rolled sheets of about 80 mils in thickness, from which tensile test specimens and coupons were machined. The samples were then solution heat treated in argon atmosphere at 1100°C for two hours followed by rapid water quenching. It should be noted here that a high quenching rate was very important, as, otherwise, the Ms temperature could be raised above room temperature due to the precipitation of Ni<sub>3</sub>Ti. Aging treatments were performed at 300°C, 500°C and 600°C for various periods of time. Subzero temperature cooling was done in liquid nitrogen (LN), and a mixture of liquid nitrogen and methyl alcohol (LNA) at about -100°C.

C. Physical Measurements

Both Rockwell-C hardness and Vickers micro-hardness measurements were performed on all specimens, except some specimens in alloy Type II where they were too soft for R-C measurement. The use of micro-hardness was to ensure there was no transformation of the metastable austenite to martensite by indentation.

Tensile tests were carried out on an Instron machine with a cross-head speed of 0.05 cm/min.

The martensitic transformation temperature was measured by differential thermal analysis, where the apparatus used was very similar to that of Goldman, et al.<sup>16</sup> The amounts of austenite and martensites were determined by x-ray analysis as described previously.<sup>15,17-19</sup>

#### D. Metallography

Specimens were examined in a Carl Zeiss optical microscope. Thin foils for transmission electron microscopy were prepared by electropolishing in the well-known chromic acid-acetic acid solution after initial chemical thinning in a hydrogen peroxide bath. A Siemens 100 kV electron microscope was used and dark field and diffraction analyses were routinely performed particularly to avoid ambiguities in interpretation of multiphased structures.<sup>20</sup>

Fractography was carried out directly in a FEL U3 scanning electron microscope operated at 25 kV.

### III. RESULTS

#### A. Martensitic Transformation Temperatures

##### (1) Type I alloy:

The Ms temperature of the as-deformed austenite was found to be about  $-85^{\circ}\text{C}$ . However, after the annealing treatments of the metastable austenite, the Ms temperatures were raised, fig. 1. This was shown by electron microscopy to be due to carbide precipitation. After  $600^{\circ}\text{C}/500$  hour annealing, the specimens were rendered essentially martensitic. From the data of fig. 1, it was possible to calculate the activation energy for this precipitation process, which was  $\sim 60$  k cal/mole. This value is of the right order of magnitude for diffusion of substitutional

solute atoms in  $\gamma$  iron, and is also very close to the value reported by Thomas, et al.<sup>1</sup> from analyses of the Portevin-Le Chatelier effect in this alloy.

(2) Type II alloy:

As in the case of Type I, Ms temperatures were generally raised as a result of precipitation. However, after 500°C/1 hour aging, the Ms temperature was found to be lowered from ~ -60°C (the unaged austenite) to ~ -90°C, and consequently, the amount of martensitic phase transformed was smaller as detected by x-ray diffraction analysis. A possible explanation for the decrease in Ms temperature will be given in a later section.

Fig. 2 gives the volume fraction of martensite determined by x-ray analysis, with different thermal treatments. Curve "a" shows the amount of martensite increasing almost linearly with time during annealing the austenite after a certain "incubation" period -- beyond which the Ms temperatures were above room temperature. Curves "b" and "c" both show an initial decrease and then a small but steady increase in the amount of martensite. As mentioned earlier, there was a lowering in Ms temperature at this particular annealing stage which can accordingly account for the lowered  $\alpha$  amount.

B. Mechanical Properties

(1) Type I alloy:

The results are shown in fig. 3. Fig. 3(b) shows the results of 0.2% flow stress of the martensite and in the case of austenitic condition, the upper yield stress. It is seen that there was a drop in yield stress upon annealing the deformed austenite. However, for

the LN quenched martensitic specimens, the variations in flow stress are characteristic of the precipitation-hardenable alloys. This is a very interesting point and will be treated in a later discussion. Tensile strength values (UTS) are also plotted vs. annealing time in fig. 3(c). It appears that the strength levels increase on annealing the deformed austenite. This is due to the formation of strain-induced martensite as confirmed by its microstructure. Elongation curves for 2 cm gauge length of the specimens are given in fig. 3(d). It is seen that the as-deformed austenite has a very high elongation (55%) and, as the annealing progressed, the elongation values drop rather drastically, whereas the elongation values for the LN cooled specimens do not behave similarly to their "parent" phase, i.e., the curves are rather flat initially and decline very slowly at longer annealing time.

There are some other interesting features regarding the tensile properties. Firstly, there was a pronounced yield drop on the stress-strain curves for the as-deformed austenitic specimens, and this yield drop decreased in magnitude upon annealing at temperatures where the mechanical properties showed significant changes, e.g. 600°C. Secondly, after several percent of straining the austenitic specimens, serrations appeared on the stress-strain curves, and an audible click sound could be heard. This phenomenon is neither due to the Portelin-Le Chatelier effect as the testing temperature was too low (room temperature) to account for it, nor due to mechanical twinning of the austenite as the product phase was ferromagnetic. Therefore, the serrations must be the result of formation of martensite during

straining. Thirdly, for the austenitic specimens, if the difference in strength values of the UTS and yield stress is indicative of the amount of work hardening, then from fig. 4 it is seen that there is a linear increase in the amount of work hardening ( $\Delta\sigma_{WH}$ ) with annealing time. The abrupt change in  $\Delta\sigma_{WH}$  signifies the occurrence of a two-phase mixture. Fourthly, the difference in flow stress values of martensitic specimens with those of the corresponding austenitic specimens may be taken as an indication of the contribution due to martensitic transformation, i.e.,  $\Delta\sigma_{MT}$ . Again, it appears that  $\Delta\sigma_{MT}$  is linearly increased with the annealing time (fig. 5), which implies precipitation on annealing may enhance the strengthening effect of the martensitic transformation.

(2) Type II alloy:

Microhardness values and tensile properties of this alloy in austenitic and martensitic conditions at different thermal treatments are shown in fig. 6(a), (b), (c), and (d). Dotted lines in fig. 6(b) represent the behavior of mixed phases. It is evident that significant changes in mechanical properties were obtained only after 500°C annealing. For this reason, a detailed study of this alloy was done particularly at this temperature. Fig. 7(a) gives the variations in tensile properties with different isothermal annealing times. Fig. 7(b) shows the strengthening effect resulting from tensile deformation,  $\Delta\sigma_{WH}$  (due to strain induced martensite), and  $\Delta\sigma_{MT}$  (due to martensitic transformation) as a function of prior austenite annealing time. It is noted that there is a definite increase of  $\Delta\sigma$  values in both cases.

A comparison between the tensile behavior of this alloy with

that of type I was also very interesting, see fig. 8. Firstly, there was no yield drop at the onset of plastic deformation, and the deviation from linearity on the stress-strain curve occurred at much lower stress than that of Alloy type I. Secondly, there was essentially no or undetectable serration on the stress-strain curves in the work hardening region. Thirdly, a higher work hardening rate was exhibited for this alloy as compared with that of type I alloy [fig. 8 curves (1) and (3); (2) and (4)].

Finally, it is noted that the stress-strain curves of the as-annealed two-phase-mixture specimens were very similar to those of the LN cooled specimens, except in the case of type I alloy, where serrations appeared on the stress-strain curves just before necking occurred.

### C. Metallography

#### (1) Type I alloy:

##### a. Microstructure of Austenite:

The microstructure of the deformed (30% rolled at 500°C) austenite, has been shown previously<sup>1,2</sup> and this investigation confirmed the earlier results that the austenite contains very fine carbide particles, which cannot be uniquely identified by electron diffraction, in addition to dense dislocation tangles.

Upon annealing at 600°C the dislocations have a tendency to arrange themselves into elongated cells of various sizes, approximately parallel to  $\langle 110 \rangle$ , and the dislocation density in the cell walls is very high (fig. 9). Dark field analysis showed the particle size to be about 80Å.

b. Microstructure of Martensite:

The microstructural features of the martensite phase obtained by LN cooling of the unannealed deformed austenite have also been published before.<sup>1,2</sup> The microstructure of martensite formed by LN cooling after annealing the 30% deformed austenite at 600°C/ 7 hrs is shown in figs. 10a, b. Generally, a finer martensite grain size was observed (as was also found by light microscopy) (fig. 10a), and the martensitic crystals seem to arrange themselves, or self-accommodate, in approximately the same orientation (fig. 10a). Figure 10b shows a dark field image of a 002 matrix reflection which includes a carbide spot and thus reveals the fine precipitates, ( $\sim 80\text{\AA}$ ).

It is interesting to examine the martensitic structure when the parent austenitic phase contains sizable precipitates, say 200 - 300 $\text{\AA}$ . However, in order to obtain this, long annealing times at 600°C, e.g., 42-1/2 hours are required. Unfortunately then the austenitic alloy transforms to martensite on cooling to room temperature, hence it was not possible to retain enough austenite to reveal its precipitation hardened structure. The presence of precipitates caused the martensitic boundaries to be irregular and less well-defined.

The carbide was identified by electron diffraction, and Table II lists the results of the "d" spacings from several diffraction patterns. Within the limit of electron diffraction, the precipitates are identified as  $\beta\text{-Mo}_2\text{C}$ , a hexagonal close-packed phase. These precipitates are arranged in Widmanstatten patterns as shown clearly

in dark field, (fig. 11). Also, the morphology of the precipitates appears to be ellipsoidal plates or rod-like, as seen from the micrograph. The orientation relationship between the matrix, in this case, martensite and  $\text{Mo}_2\text{C}$  rods is very interesting. The crystallographic features of hexagonal phase, e.g.  $\beta\text{-Mo}_2\text{C}$  and  $\epsilon$ -carbides in bcc matrix are well documented.<sup>21</sup> Two different orientation relationships differing by a rotation of  $5^\circ$  in the basal plane of the h.c.p. phase) have been established thus far. The one given by Pitsch-Schrader<sup>22</sup> showed that:

$$(011)_\alpha // (0001)_{\text{Mo}_2\text{C}}$$

$$(100)_\alpha // (2\bar{1}\bar{1}0)_{\text{Mo}_2\text{C}}$$

$$[100]_\alpha // [2\bar{1}\bar{1}0]_{\text{Mo}_2\text{C}}$$

with the  $[100]_\alpha$  being the growth direction of the  $\text{Mo}_2\text{C}$  carbides. The other relationship due to Jack<sup>23</sup> on  $\epsilon$ -carbide in tempered martensite is:

$$(011)_\alpha // (0001)_\epsilon$$

$$(101)_\alpha // (1\bar{1}01)_\epsilon$$

$$[1\bar{1}1]_\alpha // [1\bar{2}10]_\epsilon$$

and is identical to the case of hcp  $\text{Ni}_3\text{Ti}$  precipitation in martensite in maraging steels.<sup>24</sup> For the present alloy, fig. 12 reveals that the orientation relationship by Jack is obeyed. This is not surprising because the precipitates must have formed already in austenite during annealing. ( $M_s$  temperature estimated by extrapolating in fig. 1 is found to be  $\sim 50^\circ\text{C}$  up to this stage of annealing). Upon transforming to martensite, the precipitates were not likely to be sheared because of their large size, and thus the observed orientation relationship should reflect a relationship between the precipitates and the matrix

before phase transformation, i.e., the austenitic phase. Because of the close lattice match between fcc austenite and hcp precipitates, it is expected that:

$$(111)_{\gamma} // (0001)_{\text{hcp}}$$

$$[\bar{1}\bar{1}0]_{\gamma} // [1\bar{2}10]_{\text{hcp}}$$

whereas if the austenite transforms to martensite obeying the K-S relationship, namely,

$$(111)_{\alpha} // (011)_{\alpha}$$

$$[\bar{1}\bar{1}0]_{\alpha} // [\bar{1}\bar{1}1]_{\alpha}$$

as orientation relationship identical to the present result can be obtained. Similar results were also obtained recently in isothermal decomposition of a Mo austenitic alloy.<sup>25</sup>

Aging for longer periods, e.g. 600°C/600 hours, produced considerable coarsening (~1000 - 2000Å), as shown in fig. 13. There was no orientation relationship and the precipitates were identified by selected area electron diffraction to be Fe<sub>2</sub>MoC, an orthorhombic phase. Previous work on overaging reactions of Mo containing ferritic alloy steels<sup>26</sup> has shown that if the Mo/C ratio is more than about 20, the intermediate carbides M<sub>23</sub>C<sub>6</sub> and M<sub>a</sub>C<sub>b</sub> form after Mo<sub>2</sub>C and before M<sub>6</sub>C and MoC. In the present case, the Mo/C ratio is about 17 which indicates that the above rule might be applied to the austenitic phase as well.

(2) Type II alloy:

a. Microstructure of Austenite:

Austenitic specimens annealed 500°C for one hour showed a structure

which was mostly austenite.\* This means that the austenite was rendered more stable by the annealing treatment as shown by the fact that the Ms temperature of the alloy at this stage of annealing treatment was lowered. Fig. 14 shows the typical microstructure consisting of very fine spherical particles. Precipitation in this system, viz. Fe-Ni-Ti, and age-hardenable stainless steels have been studied quite extensively in view of their good high temperature mechanical properties.<sup>11,28,29</sup> It has been shown that hardening in these alloys is due to the precipitation of metastable  $\gamma'$  particles, which are coherent with the matrix of composition and possess the  $\text{Cu}_3\text{Au}(\text{L1}_2)$  ordered crystal structure. Coherency strain contrast was not detected probably because the strain is very small. This is in contrast to the similar age hardening Ni-Ti superalloys, where the lattice misfit between the  $\gamma'$  and matrix is large enough to reveal the coherency strain contrast, and the shape of the particles is cuboidal.<sup>30</sup> The particles seem to have a tendency to line up in approximately  $\langle 110 \rangle_{\gamma}$ .

After 3 hours annealing at 500°C, the structure was partially martensitic and hence will be treated in the next section.

b. Microstructure of Martensite:

For the sake of clarity, this section will be divided into two groups, namely, (i) transformation of martensite by ausaging only, (ii) further transformation by LN cooling.

(i) Transformation by ausaging:

Figure 15 shows the structure after 500°C/3 hours annealing

---

\* These alloys spontaneously transform to martensite on thinning of foils for electron microscopy. Similar results were found by Garwood and Jones.<sup>27</sup>

treatment; the bright field image (a) clearly reveals the spherical particles, martensite plate "M" and aligned particles at "A;" the selected area diffraction pattern (c) indicates a K-S relationship between martensite and the precipitates, and superlattice diffraction spots within the circled area. However, another area of the same foil shows that the orientation relationship between the matrix (bcc) and the fcc precipitates is N-W, namely  $(110)_m // (100)_p$ ,  $[1\bar{1}2] // [011]_p$ , as seen in Fig. 15(d), as was also reported for stress induced martensite in 304 stainless steel.<sup>31</sup> In some regions of the foil, discontinuous or cellular precipitation of hcpNi<sub>3</sub>Ti could be seen adjacent to the grain boundaries. The orientation relationship between the martensite matrix and the lamellar precipitates was identified by electron diffraction to be:

$$(0001)Ni_3Ti // (011)_\alpha$$

$$[1\bar{2}10]Ni_3Ti // [1\bar{1}1]_\alpha$$

i.e., the Jack relationship,<sup>23</sup> which also reflects the original relationship of the hcp precipitate with the fcc austenitic matrix lattices being closest matching. This type of boundary precipitation is generally known to be very detrimental to the ductility of the material as evidenced by the low elongation value at this stage. Longer time annealing at 500°C causes the growth of the spherical particles, cellular precipitates, and the zig-zagged martensite crystals.

(ii) Transformation by LN cooling:

The micrographs of LN cooled unannealed austenite show the sub-structure typical of low-carbon, or dislocated lath martensite (Fig. 16).

Figure 17 shows the structure after quenching to LN following aging 1 hr. at 500°C. It is seen that the grains are irregular and finer than those in Fig. 16, presumably due to the presence of fine precipitates. Fine scale {112} twins are also visible.

c. The Growth of  $\gamma'$ :

The growth of  $\gamma'$  particles in Ni-base superalloys has been studied in detail over the past decade, see e.g. Ardell.<sup>30</sup> It is generally recognized now that the growth of  $\gamma'$  particles is by diffusion-controlled coarsening. Figure 18 shows a plot of particle radius vs. (annealing time)<sup>1/3</sup>. Although there are only three data points it is seen that a straight line is obtained in accordance with the Lifshitz-Wagner relation for Ostwald ripening (see e.g. Ref. 32).

#### IV. DISCUSSION

##### 1. Effect of Austenite Structure on Martensite

One of the objectives of the experiments was to try to establish that precipitates and not dislocations introduced into austenite prior to transformation are effective in increasing the strength. As shown by Fig. 3 although softening of ausformed austenite occurs by annealing, the corresponding martensite increases in strength. The two microstructural effects occurring after aging the ausformed austenite are: 1) dislocation recovery and 2) precipitation hardening. Thus, in austenite the effects of precipitates override the effects of dislocations on the subsequent strength of martensite. There are several ways in which precipitates can be thus effective as discussed below.

Consider the effect of particles in the austenite on the structure of transformed martensite. If we consider the martensitic transformation as a special kind of plastic deformation, then the problem becomes

very similar to the case of studying work-hardening behavior of a dispersion-hardened crystal,<sup>33</sup> except the latter does not involve a change in crystal structure. For the case of martensitic transformation, a simplified schematic model in Fig. 19 may help to illustrate the role of particles.

Either the particles deform with the matrix during the  $\gamma \rightarrow M_s$  transformation as is expected in alloy 2 or, if the particles are rigid, then rearrangement of the mass at the particle-matrix interface must occur by plastic deformation (e.g. prismatic punching). The latter is expected for the  $Mo_2C$  precipitates in alloy 1. In this case a much higher dislocation density will be expected in the final martensite and on plastic deformation a greater work-hardening capacity is obtained as a result of mobile dislocation - particle interactions (for review see e.g. Ref. 33).

The presence of precipitates in the metastable austenite usually will tend to promote the formation of martensite by providing suitable nucleating sites, because (a) chemically, regions in the vicinity of precipitates are known to be solute-atom depleted and hence are energetically more stable with respect to martensitic phase, i.e. they are potential areas for the formation of martensite once the driving force for transformation is large enough, and (b) mechanically, precipitates will either elastically strain the surrounding austenitic matrix or cause plastic flow in the matrix near the precipitates. This effect may stabilize the austenite or favor martensite nucleation depending on the nature of the strains involved. From this work, however, it appears that precipitates favor nucleation so that it should be possible to obtain a more or less controlled and uniform distribution of martensite

phase by transforming a dispersion hardened austenitic phase.

Because of the compatibility and continuity between lattices of the martensite phase and austenitic matrix, the latter must be plastically deformed by the growing martensite crystals. Since a dispersion hardened austenite has a higher flow stress than the single-phase austenite, we may expect that the growth of martensite crystals in the strengthened austenitic matrix must be impeded to some extent. The result is that the martensite grain size tends to be smaller and the arrangement of martensite crystals may be in such a way that they grow only on certain crystallographic habit planes and/or be self-accommodated in bundles in order to minimize the resultant strain energy of the system. Christian<sup>34</sup> suggests that if the coherency of the glissile interface is lost (e.g. as a result of deformation), this will lead to stabilization.

Hornbogen and Meyer<sup>35</sup> found a decrease in  $M_s$  temperature of a  $\gamma'$  precipitated austenite after short aging times at 600°C and they attributed this effect to the shearing of the f.c.c. precipitate to a b.c.c. structure when the austenite was transformed to martensite. Presumably excess energy was required to shear these particles to a new crystal structure. A similar effect, i.e., lowering in  $M_s$  temperature, was also obtained in alloy 2 here, so that it is very interesting to examine how a fine coherent precipitate in austenite can alter the value of free energy change when the austenite-martensite transformation occurs.

Consider a homogeneous austenitic solid solution with a  $M_s$  temperature and total driving force or free energy change  $\Delta G_s$  for martensitic transformation,  $M_s$  and  $T_0$  [the equilibrium temperature at

which free energies of austenite and martensite are equal, approximately taken as  $1/2 (A_s + M_s)$ ] are usually known to increase with decreasing amounts of solute whereas the measurement of  $\Delta G_s$  is generally taken as the magnitude of  $(T_o - M_s)$ , and hence decreases moderately with decreasing solute concentration. With this fact in mind, consider the annealing or aging effect of the alloy. As soon as precipitation occurs, because of the solute atom depletion from the matrix, the  $M_s$  temperature is raised and  $\Delta G_s$  reduced in the manner described above. But in addition to this change in properties of the matrix, the effect of precipitation per se must be considered. Two possibilities may occur when the austenite containing fine coherent f.c.c. precipitates transforms to martensite:

- (1) the precipitates are deformed or sheared in conforming with the surrounding austenitic matrix.
- (2) the precipitates are not sheared during martensitic transformation of the austenite.

These two alternatives are shown schematically in Fig. 19, where the martensitic transformation is simulated by a simple homogeneous shear. The possibility (1) would involve the energy consumed to allow for the shearing of the precipitates, whereas the possibility (2) would require the rearrangement of the mass surrounding the particles which essentially creates a high energy incoherent interface between the matrix and particles. Thus, the final effect will be determined by the balance of these two possibilities. If we take the radius of the precipitates as  $r$ , the number of precipitates per unit volume as  $N$ , the high energy interfacial energy per unit area of the interface as  $\gamma$  and the free energy needed to shear the precipitates per unit volume of the deformed precipitate as  $\Delta G_v$ , then the free energy change for possibility (1) is

$$\Delta G_1 = \frac{4}{3} \pi N r^3 (\Delta G_v) \text{ and for possibility (2), } \Delta G_2 = 4 \pi N r^2 \gamma.$$

It is seen that for small values of  $r$ ,  $\Delta G_1$  is smaller than  $\Delta G_2$  and accordingly, shearing of the precipitate is preferred because the total free energy change for the system  $\Delta G_t = \Delta G_s + \Delta G_1$  would be more negative. The critical radius for the shearing of precipitates is then  $r_c = 3\gamma/\Delta G_v$  by simply equating  $\Delta G_1$  and  $\Delta G_2$ .

From the above discussion, the lowering of  $M_s$  temperature in the present study could possibly be explained as the extra driving force needed to shear the precipitates. But as the precipitates grow coarser, i.e. above  $r_c$ , where deformation of the precipitates does not occur, the raising of  $M_s$  temperature due to solute element depletion becomes overpowering and predominating over the possible decreased  $M_s$  temperature on forming incoherent interfaces on transformation. The variation in  $M_s$  temperature by precipitation has been treated in the consideration of austenite stabilization in recent years, for example, the destruction of martensite embryos by precipitation,<sup>36</sup> locking of the martensite/austenite interface by solute atom segregation,<sup>37</sup> the strengthening effect of the austenite matrix by strain-aging processes,<sup>38</sup> etc. But all the models for stabilization of austenite are concerned with the segregation of interstitial solute atoms, which is not the case in the present study. The whole argument mentioned so far could be looked upon from another point of view. The net free energy change  $\Delta G$  for martensitic transformation could be taken as analogous to the work done by stress applied to plastically deform the austenite, except the work hardened product is martensite. Then the presence of precipitates will serve to resist the plastic flow and hence the interparticle spacing  $d$

is an important parameter. Below a critical  $d_c$  value, plastic flow or transformation will not occur unless more stress or energy is added to the system. In the case of precipitation hardening by coherent particles, there exists a critical  $r_c$  radius (for a given volume fraction of precipitates) which denotes the change from a dislocation cutting mechanism to a by-pass mechanism.<sup>39</sup> The value of  $r_c$  is  $2Gb^2/\pi E$  (by equating  $\tau_c = \frac{\pi Er}{2bd}$  for cutting and  $\tau = \frac{Gb}{d}$  for by-passing), where  $E$  is the energy per unit area of the planar fault generated after cutting,  $G$  is shear modulus and  $b$  is Burgers vector. We see that  $r_c$  obtained in this way is essentially the same expression as deduced previously from free energy considerations, with  $Gb^2$  (the line tension of dislocations) corresponding to the high energy interfacial energy  $\gamma$  after martensitic transformation and  $E$  corresponding to the free energy change due to shearing of the precipitates  $\Delta G_v$ .

## 2. Mixed Phases of Martensite and Austenite

It has been shown by Mangonon and Thomas<sup>15</sup> that the yield strengths of 304 stainless steel are linearly proportional to the volume fraction of  $\alpha$  irrespective of the treatment used to form  $\alpha$ , i.e., either stress nucleated or by thermal aging. Furthermore, the strength of the above system was better described as a special kind of composite strengthening due to the fact that the hard martensite crystals were too large in size (and large interparticle spacing) to be accounted for by a dispersion hardening mechanism.

In the present case, after annealing the austenite to a certain extent, precipitation and the partial formation of martensite occurred simultaneously, and the whole system is actually composed of three phases. However, precipitation took place on a scale much finer than that of

martensite (as seen in micrographs). The latter is not likely to affect the movement of dislocations as compared to the fine precipitates during deformation, so that it is interesting to see the strengthening of both austenite and martensite on the overall behavior of the "composite." The data of type II alloy are replotted in Fig. 20. It is seen that the "law of mixtures" is still obeyed and the lines are displaced to high strength levels depending to what extent the austenite and martensite are strengthened.

## V. CONCLUSIONS

1. It is shown that although softening of the ausformed austenite occurs on annealing, the corresponding strength of the transformed martensite shows an increase. This is explained on the basis of increased dislocation density due to dislocation - particle interactions upon transformation. Hence the enhancement of substructure strengthening of martensite is made possible by pre-dispersing hard particles in the austenite, and taking advantage of the dislocations generated by the  $\gamma$ -Ms transformation.

2. It is suggested that the conventional ausforming process could possibly be modified by deforming just enough to allow nucleation of precipitation, followed by a suitable aging treatment so as to obtain optimum particle size and spacing to give the maximum dislocation density upon quenching to martensite.

3. The good ductility of the ausformed martensite could be explained by the homogeneous distribution of dislocations, refined martensite grain size, and the decreased tetragonality of martensite lattice, due to removal of carbon as  $\text{Mo}_2\text{C}$ .

4. In the ausaged alloy, the decrease in Ms temperature of the austenite containing fine coherent  $\text{Ni}_3\text{Ti}$  precipitates could be accounted for by the extra driving force needed to deform the precipitates.

5. Whether the precipitates deform with the matrix or not during martensitic transformation, there always exists a strengthening effect on the final product, although non-deformable particles are more effective, as expected.

6. Mixed phase structures can be described as "composites" with a linear relation between yield strength of the composite and volume fractions and yield strengths of the  $\gamma$  and Ms phases.

ACKNOWLEDGEMENTS

This work was supported by the United States Atomic Energy Commission through the Inorganic Materials Research Division of the Lawrence Radiation Laboratory.

1. G. Thomas, D. Schmatz and W. Gerberich, "High Strength Materials," John Wiley and Sons, New York, p. 284 (1965).
2. O. Johari and G. Thomas, ASM Trans. Quart., 58, 563 (1965).
3. L. Raymond and W. Reuter, Acta Met., 12, 948 (1964).
4. T. Araki, S. Watanabe and H. Miyaji, Proceedings of the International Conference on the Strength of Metals and Alloys, p. 111 (1967).
5. E. B. Kula and C. F. Hickey, AIME Trans. 230, 1707 (1964).
6. E. B. Kula and J. M. Dhosi, ASM Trans. 52, 321 (1960).
7. I. Tamura, Trans. JISI, Vol. 6, 249 (1966).
8. A. J. McEvily, R. H. Bush, F. W. Schaller and D. J. Schmatz, ASM Trans., 56, 753 (1963).
9. V. F. Zackay and W. M. Justusson, "High Strength Steels," special report 76, Iron and Steel Institute, p. 14 (1962).
10. R. Phillips and W. E. Buckworth, "High Strength Materials," John Wiley and Sons, New York, p. 307 (1965).
11. G. Thomas, Met. Trans. 2, 2373 (1971).
12. P. K. Pitler and G. S. Ansell, ASM Trans. 57, 220 (1964).
13. V. F. Zackay, E. R. Parker, D. Fahr and R. Busch, ASM Trans. 52, 60 (1967).
14. K. W. Andrews, JISI, 203, 721 (1965).
15. P. L. Mangonon, Jr. and G. Thomas, Met. Trans. 1, 1587-1594, 1970.
16. A. J. Goldman, W. D. Robertson and D. A. Koss, AIME Trans. 230, 240 (1964).
17. R. L. Miller, ASM Trans. 57, 892 (1964).

18. H. R. Erard, "Advances in X-ray Analysis," Plenum Press, New York, p. 256 (1963).
19. B. D. Cullity, "Elements of X-ray Diffraction," Addison-Wesley, Mass. (1956).
20. G. Thomas, I-Lin Cheng and J. R. Mihalisin, ASM Trans. Vol. 62, 852 (1969).
21. D. J. Dyson, S. R. Keown, D. Raynor and J. A. Whiteman, Acta Met. 14, 867 (1966).
22. W. Pitsch and A. Schrader, Arch. Eisenhitt Wes. 29, 715 (1958).
23. K. M. Jack JISI, 169, 26 (1951).
24. I-Lin Cheng and G. Thomas, ASM Trans. 61, 14 (1968).
25. F. G. Berry, A. T. Davenport and R. W. K. Honeycombe, "The Mechanism of Phase Transformation in Crystalline Solids," Institute of Metals, Monograph and Report Series No. 33, p. 288 (1969).
26. J. H. Woodhead and A. G. Quarrell, JISI, 203, 605 (1965).
27. R. D. Garwood and R. D. Jones, JISI, 204, 512 (1966).
28. B. R. Clark and F. B. Pickering, JISI 205, 70 (1967).
29. L. K. Singhal and J. W. Martin, Acta Met. 16, 967 (1968).
30. A. J. Ardell, Metallurgical Trans. 1, 525 (1970).
31. P. L. Mangonon, Jr. and G. Thomas, Met. Trans. 1, 1577-1586, 1970.
32. G. W. Greenwood, The Mechanism of Phase Transformations in Crystalline Solids, p. 103, Institute of Metals (London) Rep and Mon #33 (1969).
33. M. F. Ashby, Second International Conference on Strength of Metals and Alloys, American Society for Metals (1970) vol. 2, p. 507.
34. J. W. Christian, JISI Special Report 93 (London) (1965).

35. E. Hornbogen and W. Meyer, Acta Met. 15, 584 (1967).
36. K. A. Malyshev and M. M. Vasilevskaya, Physics and Metals Metallography 18, 150 (1965).
37. J. Woodilla, P. G. Winchell and M. Cohen, AIME Trans. 215, 849 (1959).
38. E. R. Morgan and T. Ko, Acta Met. 1, 36 (1953).
39. A. Kelly and R. B. Nicholson, Precipitation Hardening, Prog. Mat. Sci., 10, 151 (1963).

TABLE II

Interplanar Spacings of the Precipitates: from Alloy I

<u>Thin Foil</u>	<u>Martensite</u>	<u><math>\beta</math>-Mo<sub>2</sub>C</u>	
D(Å)	d(Å)	d(Å)	hk.l
		4.724	00.1
2.6 (P)*		2.600	01.0
2.36 (P)		2.362	00.2
2.28 (P)		2.278	01.1
2.027	2.027	2.278	01.1
1.71 (P)		1.748	01.2
		1.575	00.3
1.49 (P)		1.501	11.0
1.43, 1.43 (P)	1.433	1.431	11.1
		1.374	01.3
1.31		1.300	02.0
1.27		1.267	11.2
1.25		1.253	02.1
1.17, 1.18 (P)	1.170	1.181	00.4
		1.139	02.2
1.08 (P)		1.087	11.3
	1.013	1.075	01.4
		1.003	02.3
0.97 (P)	0.906	0.983	12.0

\* (P) means precipitate

FIGURE CAPTIONS

- Fig. 1 The variation of Ms temperature vs. annealing time for type I alloy. The rise of Ms temperature is due to depletion of Mo and C from the matrix.
- Fig. 2 Volume fraction of martensite phase vs. ausaging time for type II alloy.
- Fig. 3 Mechanical properties vs. annealing time for type I alloys. Note in (b) the yield stresses of austenite decrease gradually whereas the flow stresses of the corresponding martensite increases.
- Fig. 4  $\Delta\sigma_{WH}$  (the difference between UTS and YS vs. annealing time for type I alloys. Note that  $\Delta\sigma_{WH}$  is an increasing function of annealing time.
- Fig. 5  $\Delta\sigma_{MT}$  (the difference between yield stresses of austenite and corresponding martensite, which reflects the contribution from martensitic transformation) vs. annealing time for type I alloys.
- Fig. 6 Mechanical properties vs. annealing temperatures for type II alloys. (a), (b) are austenitic alloys whereas (c), (d) are LN cooled martensite.
- Fig. 7 Plot of tensile properties vs. ausaging time (a) and  $\Delta\sigma$  values vs. ausaging time (b) for type II alloys.

Fig. 8 Stress-strain curves for type I and type II alloys. Note the effect of prior annealing in austenite on both the yield stresses and work hardening behavior of the alloys.

Fig. 9 The structure of  $600^{\circ}\text{C}/7\text{hrs}$  annealed austenite, showing the development of dislocation cell substructures. (bright field).

Fig. 10 Dark field images of  $600^{\circ}\text{C}/7\text{hrs}$  annealed and LN cooled martensite structures (type I), showing (a) the fragmentation of martensite crystals and (b) the presence of very fine precipitates.

Fig. 11 Dark field image showing the Widmanstätten arrangement of  $\text{Mo}_3\text{C}$  precipitates in type I alloy as a result of annealing ( $600^{\circ}\text{C}/42\frac{1}{2}$  hrs. plus LN cooled).

Fig. 12. Analysis of the diffraction pattern of Fig. 11

Fig. 13 Structure of  $600^{\circ}\text{C}/600$  hrs plus LN cooled type I specimens showing the growth of carbides into spheroids. (bright field)

Fig. 14 Dark field image of the  $500^{\circ}\text{C}/1$  hr ausaged specimen (type II alloy) showing the presence of very fine precipitates.

Fig. 15  $500^{\circ}\text{C}/3$  hrs ausaged type II specimen showing (a) the diffuse martensite boundaries (bright field), (b) K-S relationship between matrix and precipitates (c) another area and (d) N-W orientation relationship.

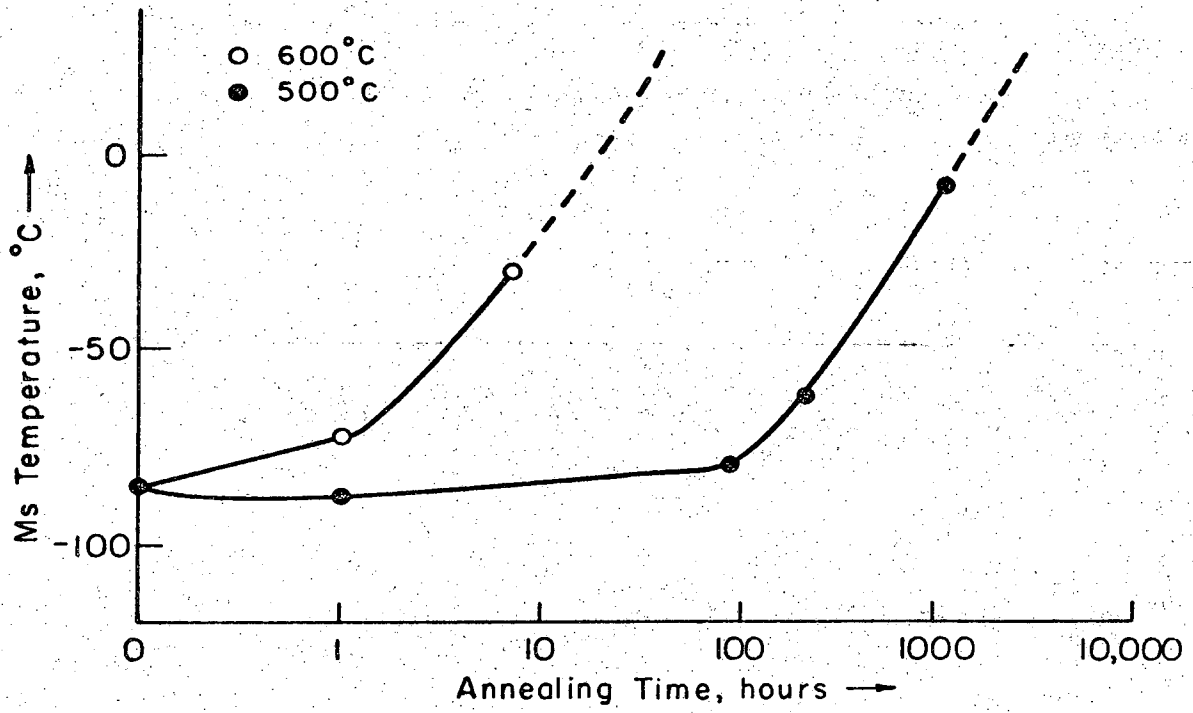
Fig. 16 Structure of LN quenched martensite (type II) alloy, showing the presence of predominately lath martensite.

Fig. 17 Dark field image of 500°C/1 hr ausaged plus LN cooled martensite, showing the distortion, refinement of martensite crystals and the presence of very fine precipitates (type II alloy).

Fig. 18 Plot of radius of precipitates vs. (ausaging time)<sup>1/3</sup> of type II alloy, showing a straight line is obtained.

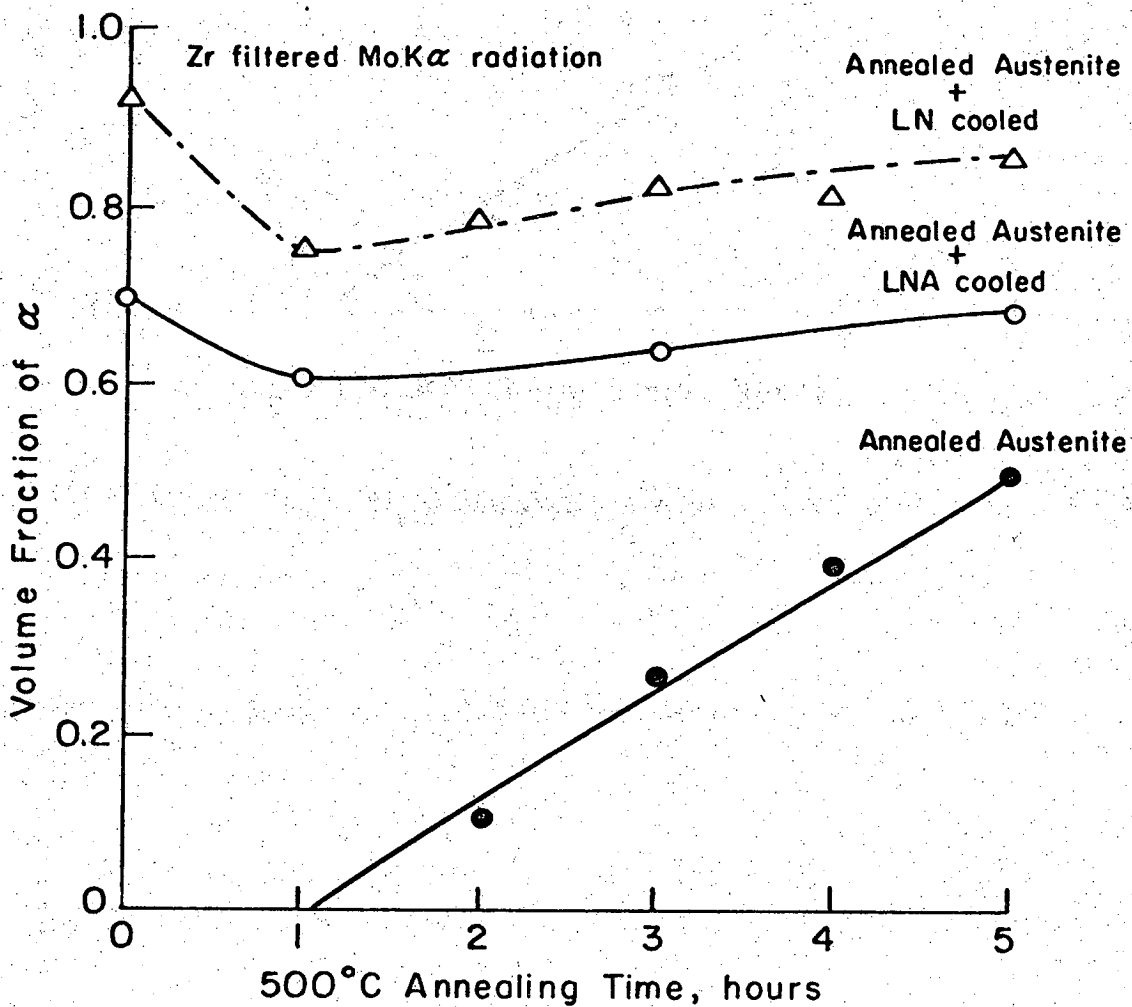
Fig. 19 Schematic description of martensitic transformation of a dispersion-hardened austenite.

Fig. 20 Plot of yield strength vs. volume fraction of martensite phase of type II alloy.



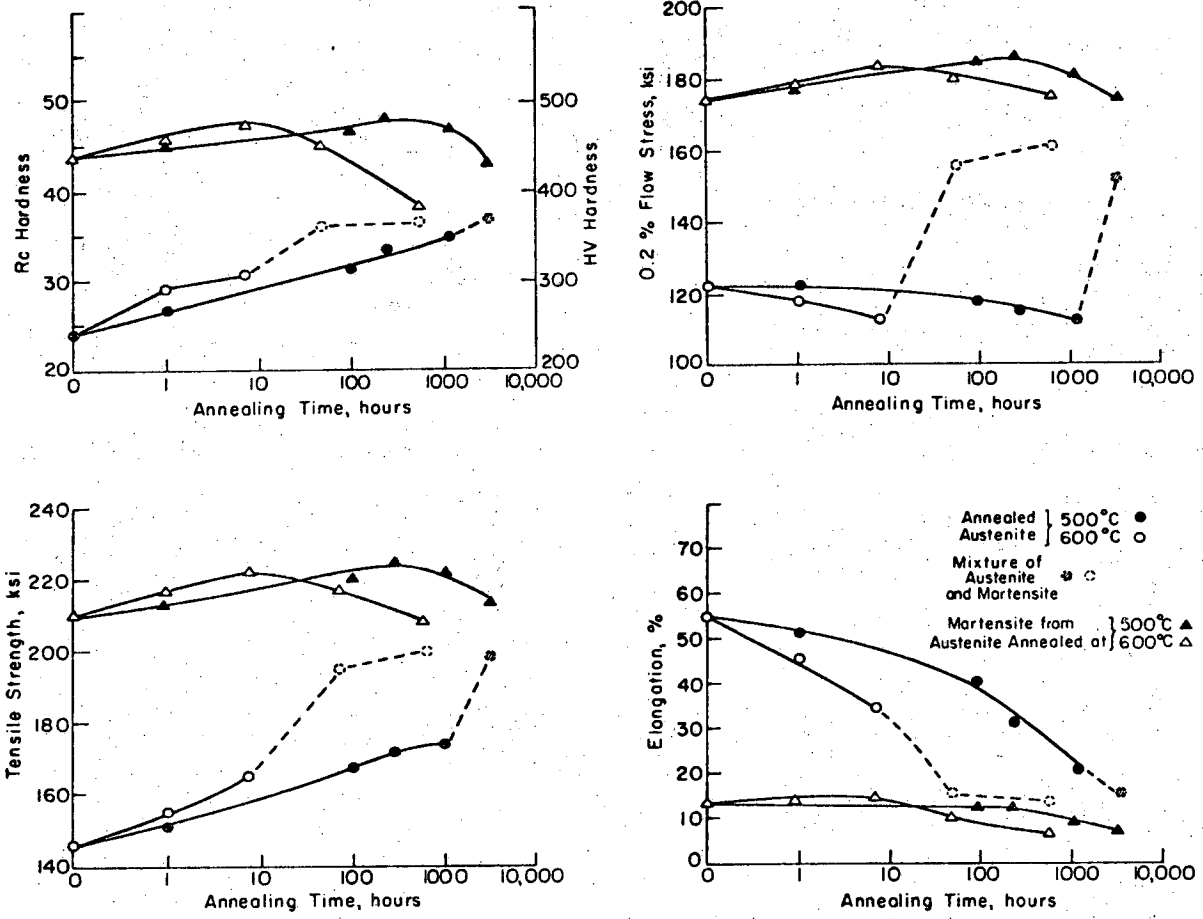
XBL 704-662

Fig. 1



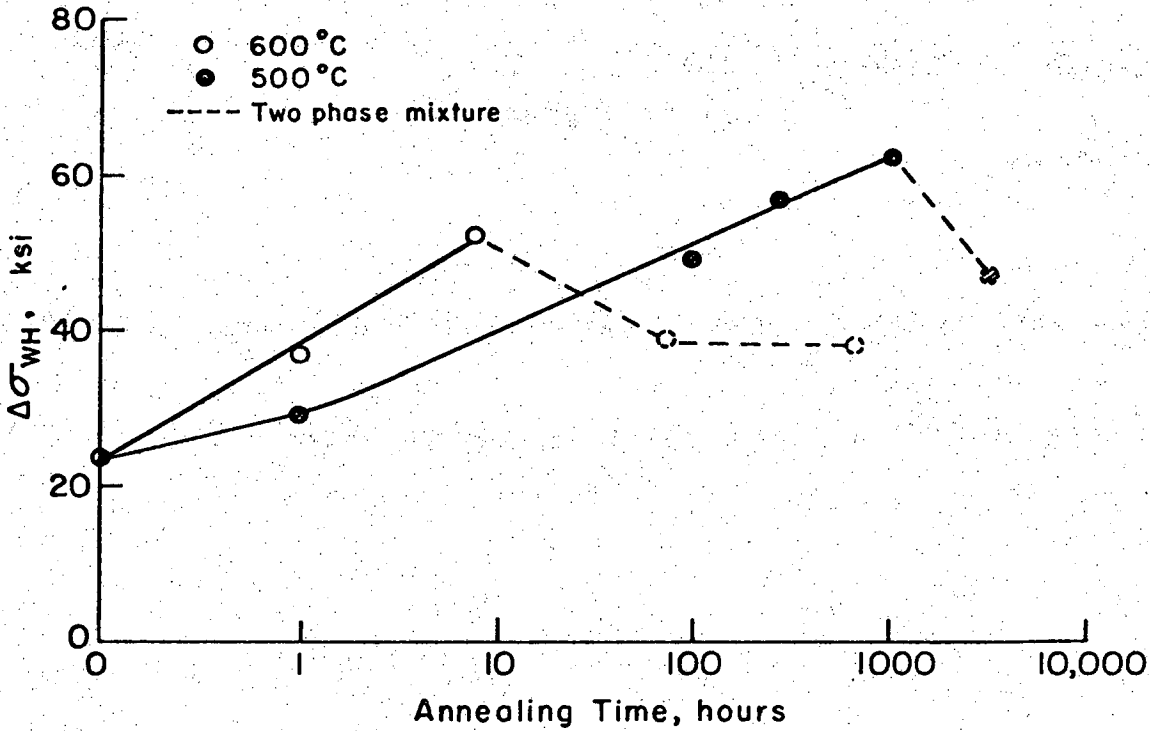
XBL 704-664

Fig. 2



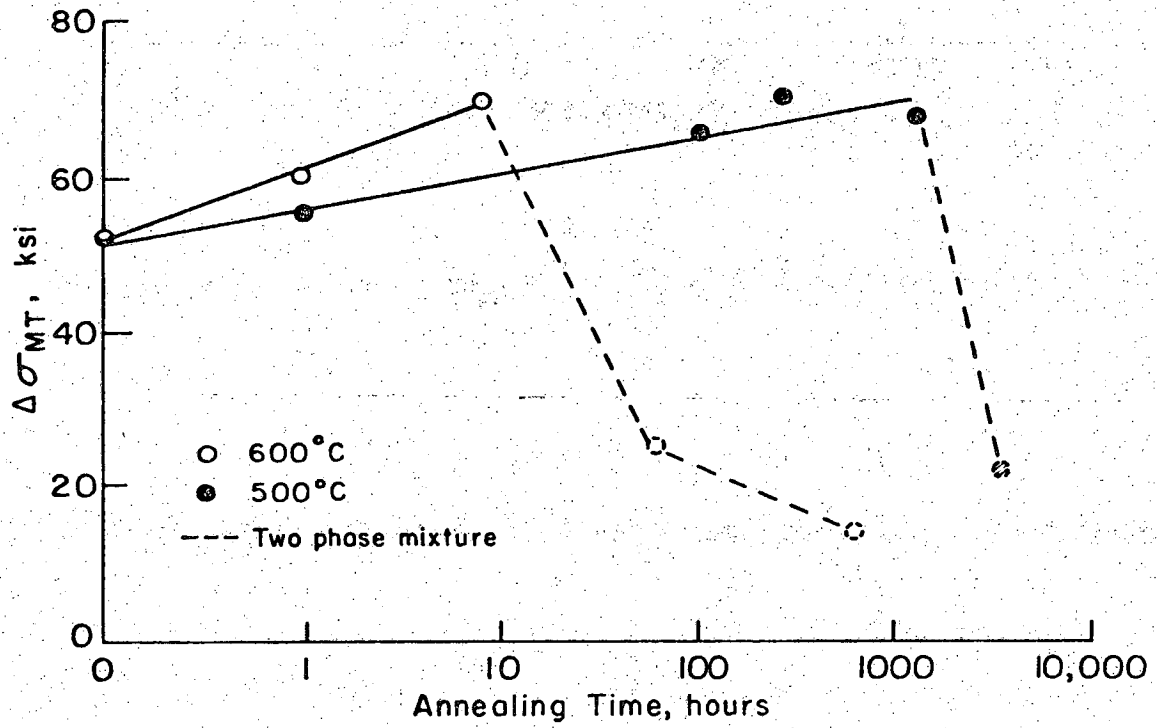
XBL 704-660

Fig. 3



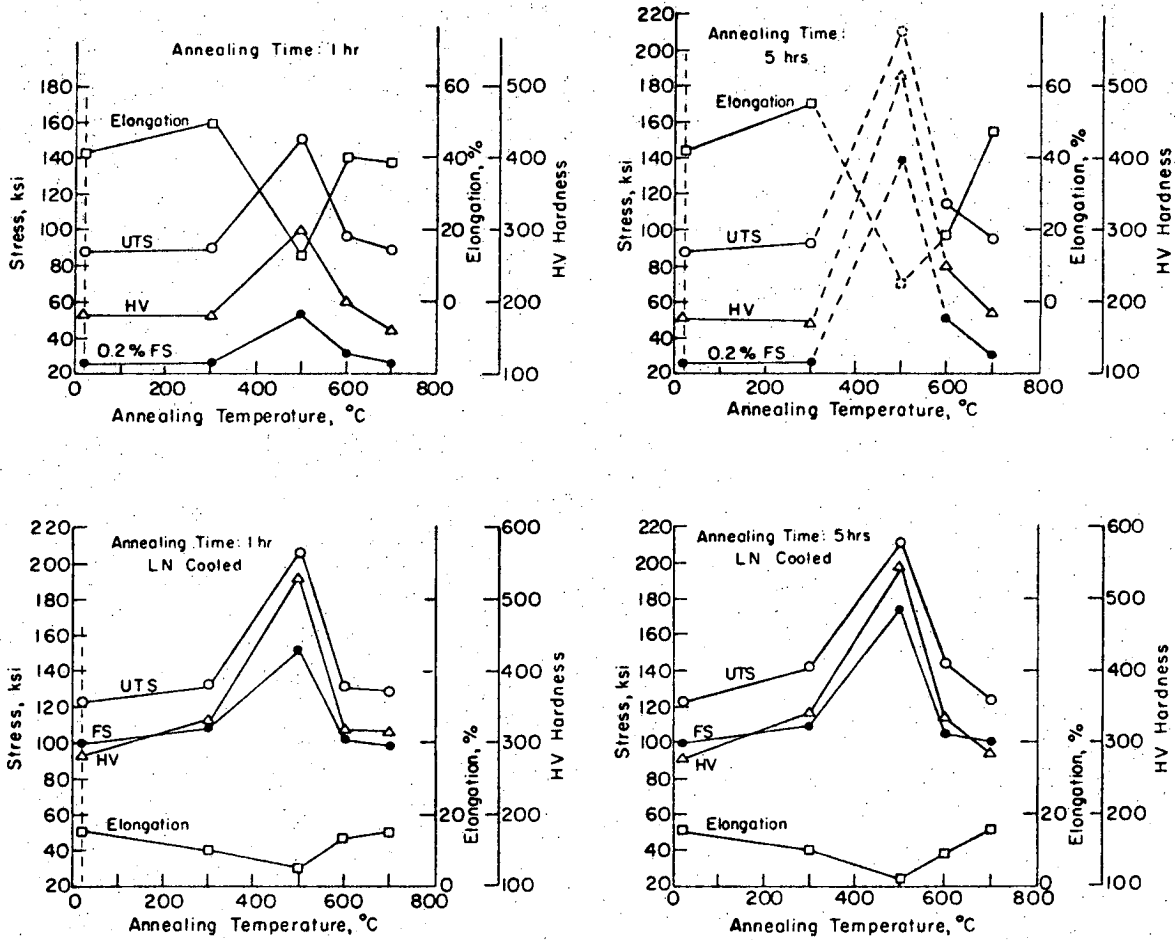
XBL 704-661

Fig. 4



XBL 704-669

Fig. 5



XBL 704-670

Fig. 6

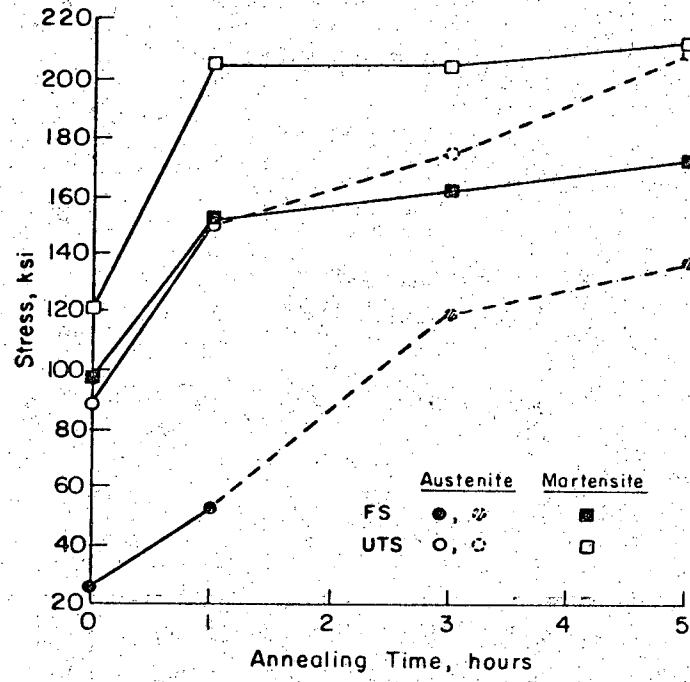
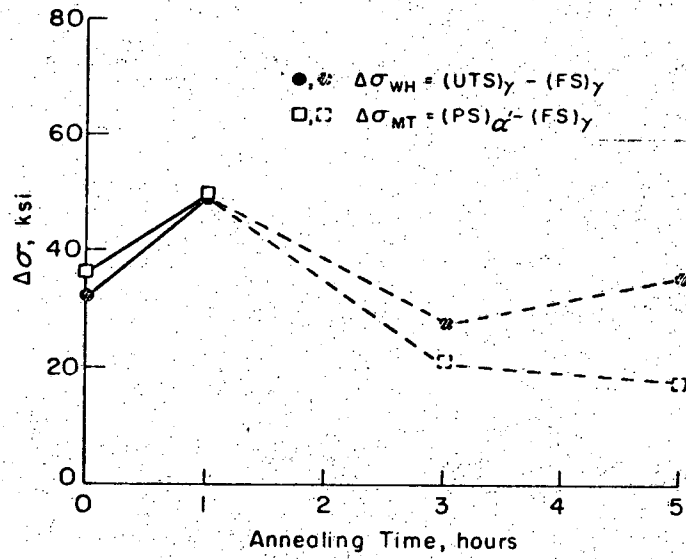
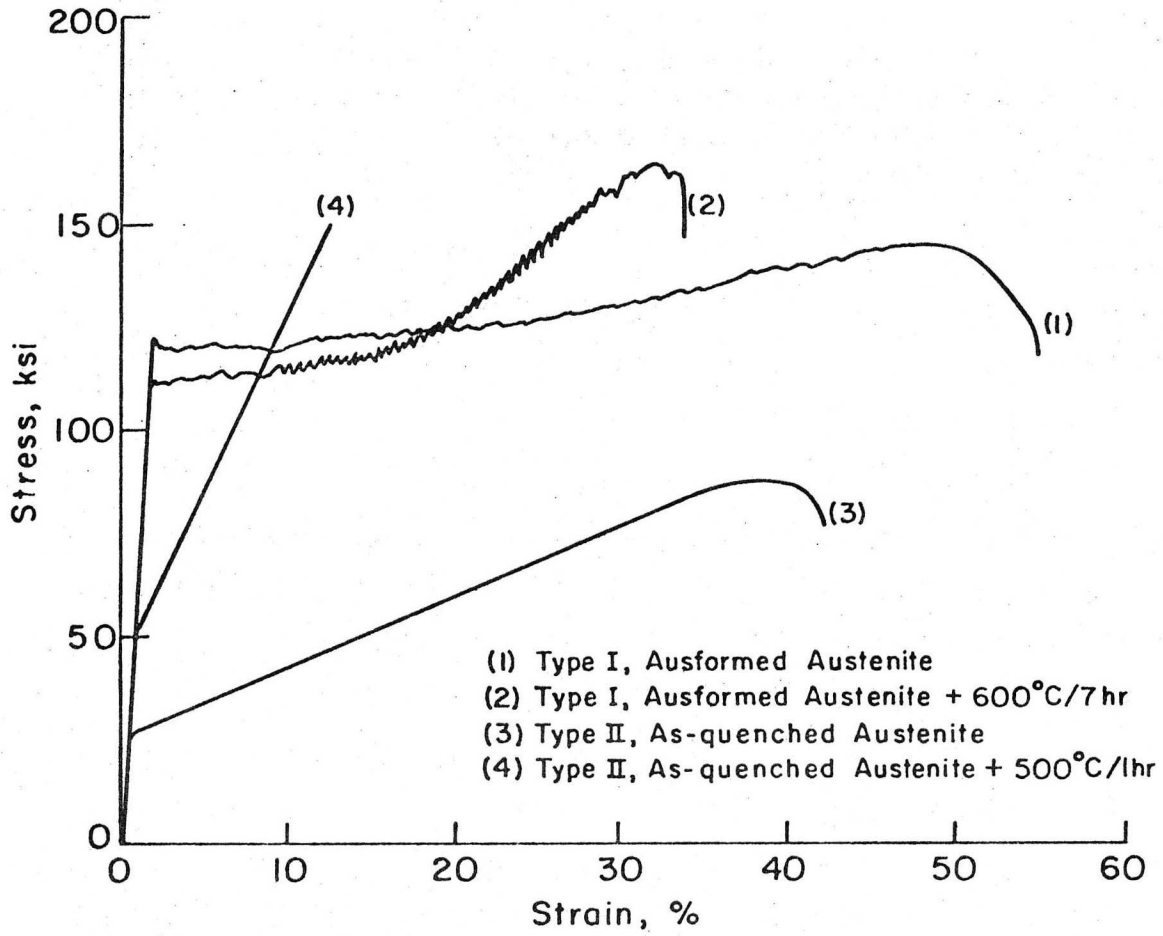


Fig. 9a



XBL 704-659

Fig. 7



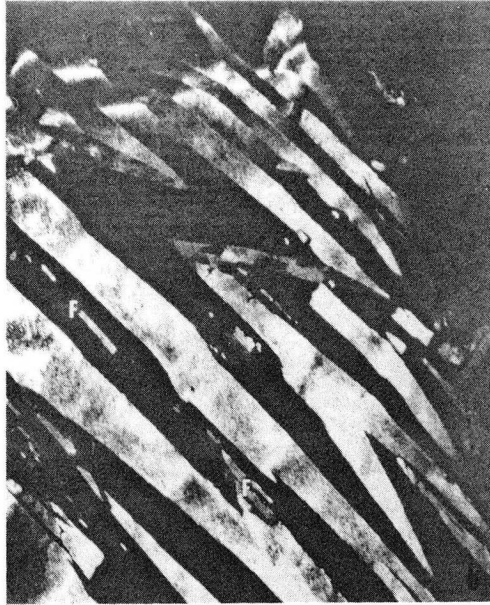
XBL 704-668

Fig. 8



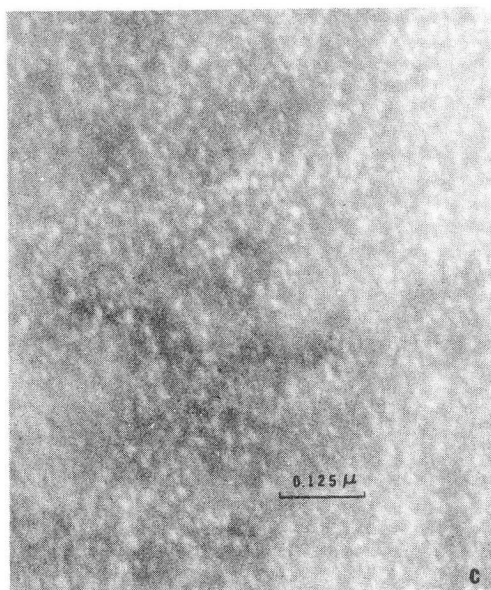
XBB 704-1543  
(lower left)

Fig. 9



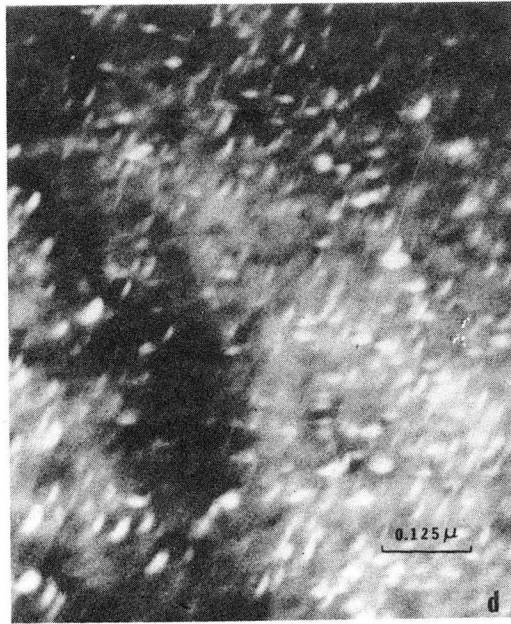
XBB 704-1547  
(upper right)

Fig. 10a



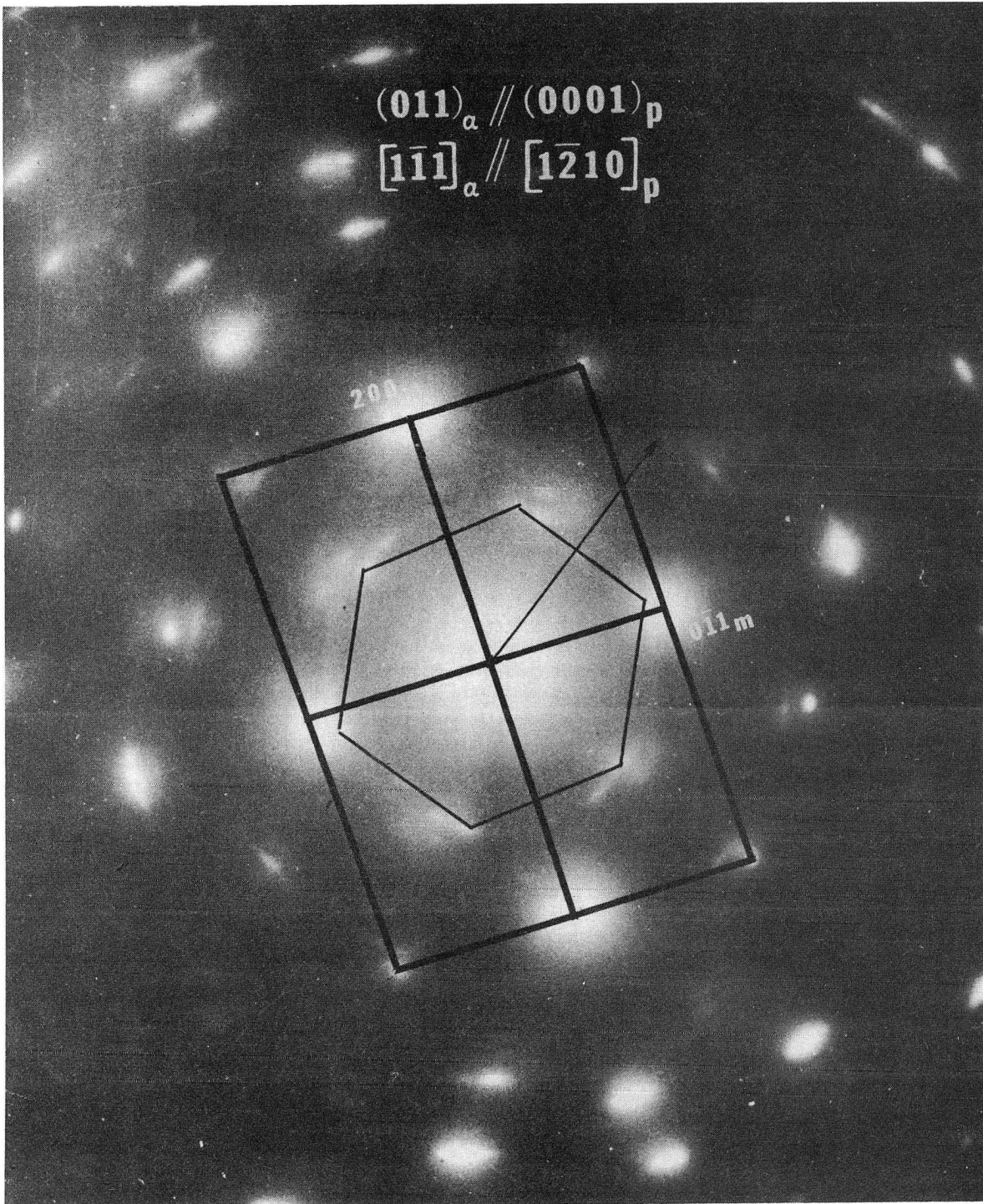
XBB 704-1544  
(bottom)

Fig. 10b



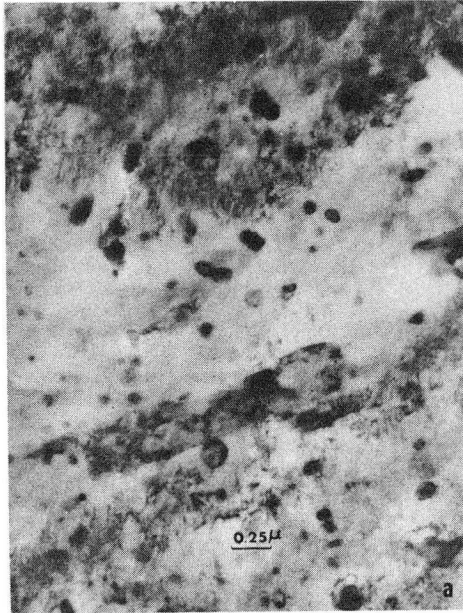
XBB 704-1542  
(lower right)

Fig. 11



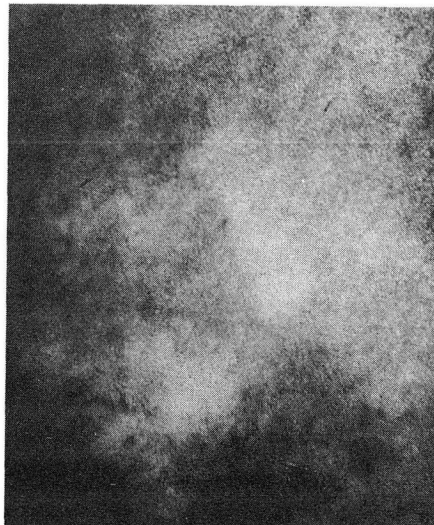
XBB 704-1550

Fig. 12



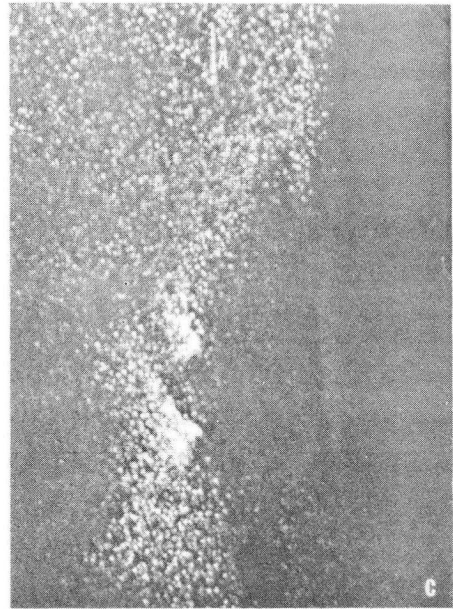
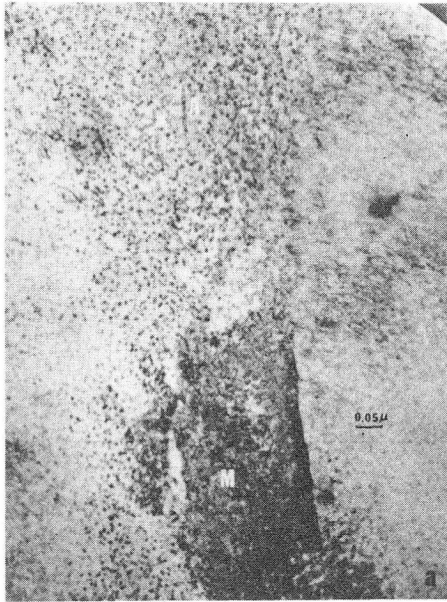
XBB 704-1554  
(right)

Fig. 13



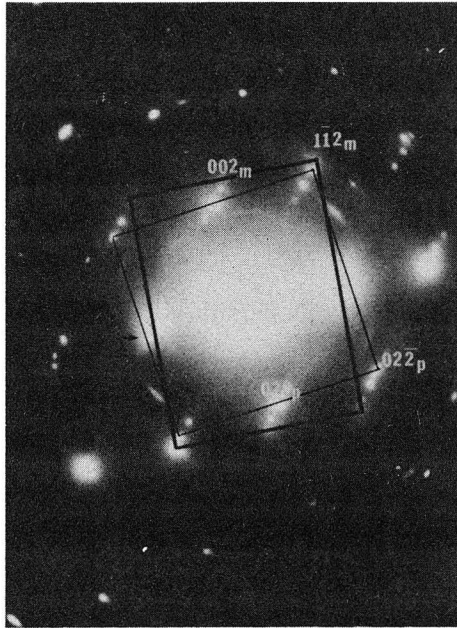
XBB 704-1558  
(upper right)

Fig. 14



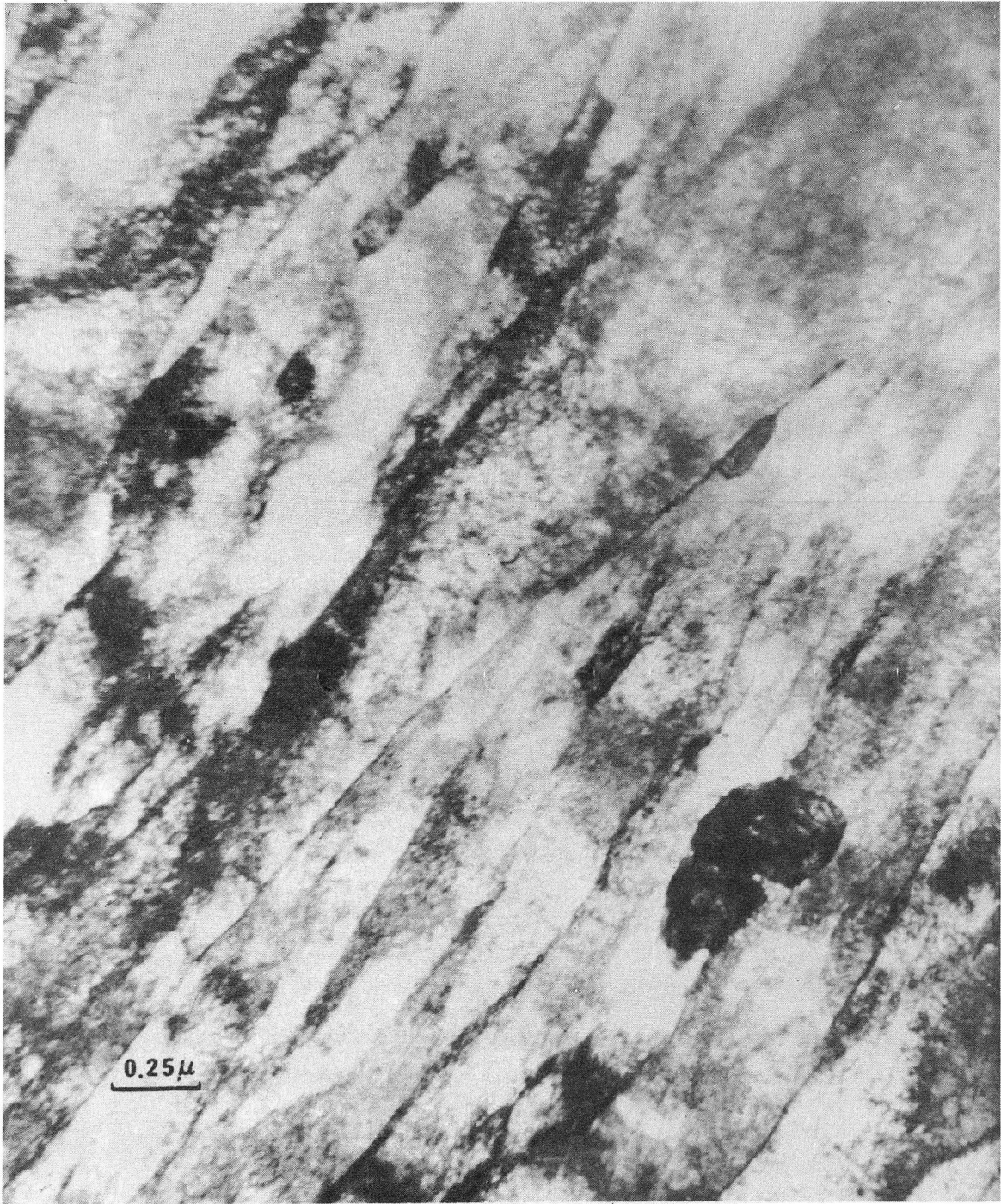
XBB 704-1553

Fig. 15



XBB 704-1548  
(bottom)

Fig. 15d



XBB 704-1561

Fig. 16



XBB 704-1539  
(bottom right)

Fig. 17

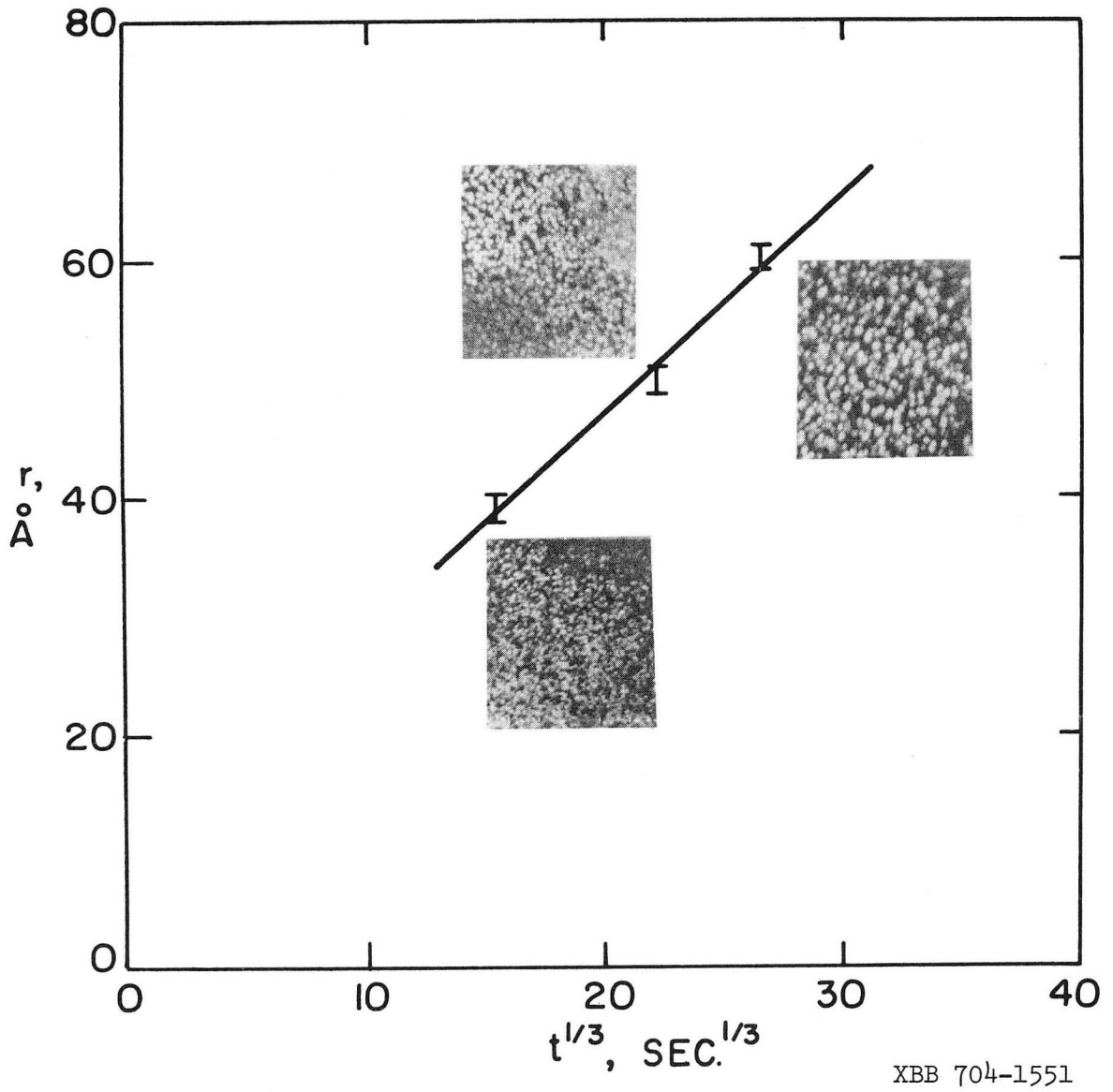
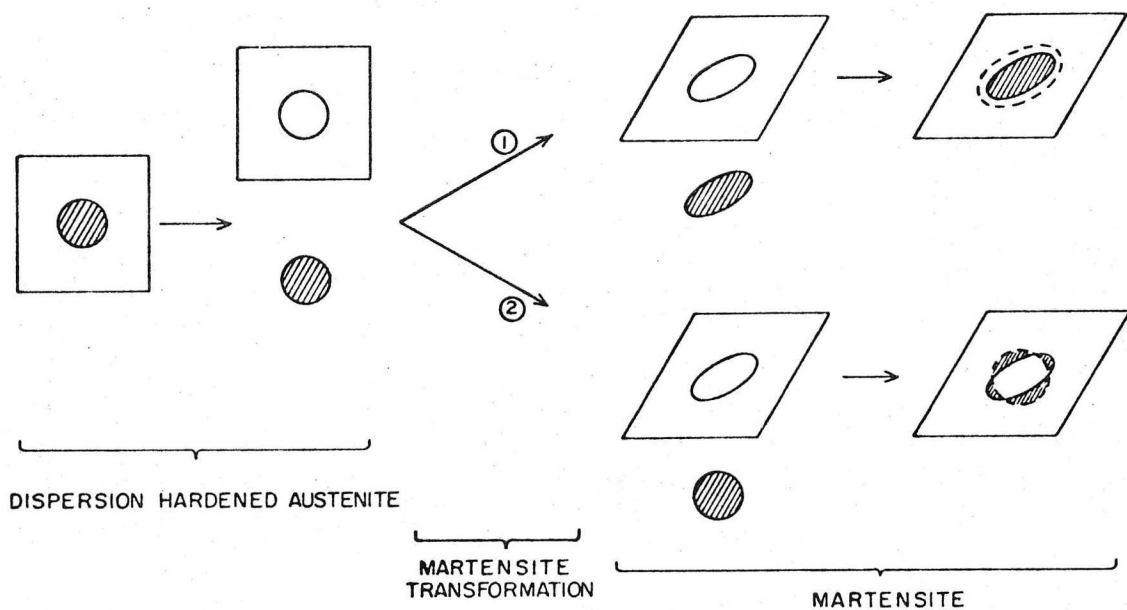
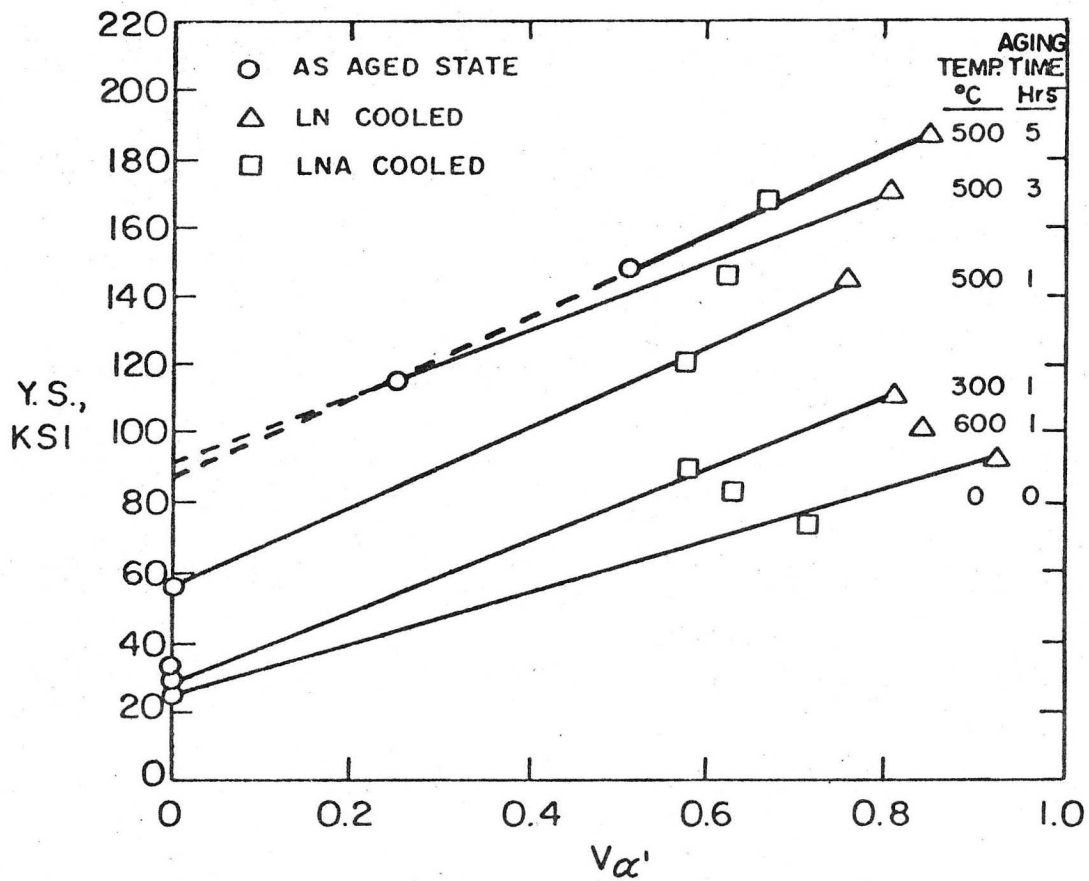


Fig. 18



XBL 704-666

Fig. 19



XBL 704-667

Fig. 20

LEGAL NOTICE

*This report was prepared as an account of work sponsored by the United States Government. Neither the United States nor the United States Atomic Energy Commission, nor any of their employees, nor any of their contractors, subcontractors, or their employees, makes any warranty, express or implied, or assumes any legal liability or responsibility for the accuracy, completeness or usefulness of any information, apparatus, product or process disclosed, or represents that its use would not infringe privately owned rights.*

TECHNICAL INFORMATION DIVISION  
LAWRENCE BERKELEY LABORATORY  
UNIVERSITY OF CALIFORNIA  
BERKELEY, CALIFORNIA 94720